

Article

# A Numerical Intuition of Activation Energy in Transient Micropolar Nanofluid Flow Configured by an Exponentially Extended Plat Surface with Thermal Radiation Effects

Zeeshan <sup>1,†</sup>, N. Ameer Ahammad <sup>2</sup>, Haroon Ur Rasheed <sup>3</sup>, Ahmed A. El-Deeb <sup>4,\*</sup> , Barakah Almarri <sup>5</sup>  and Nehad Ali Shah <sup>6,†</sup><sup>1</sup> Department of Mathematics, Bacha Khan University Charsadda, Charsadda 24420, Pakistan<sup>2</sup> Department of Mathematics, Faculty of Science, University of Tabuk, Tabuk 71491, Saudi Arabia<sup>3</sup> Department of Computer Science, Sarhad University of Science and Information Technology, Peshawar 25000, Pakistan<sup>4</sup> Department of Mathematics, Faculty of Science, Al-Azhar University, Cairo 11884, Egypt<sup>5</sup> Department of Mathematical Sciences, College of Sciences, Princess Nourah Bint Abdulrahman University, Riyadh 11671, Saudi Arabia<sup>6</sup> Department of Mechanical Engineering, Sejong University, Seoul 05006, Korea

\* Correspondence: ahmedeldeeb@azhar.edu.eg

† These authors are contributed equally to this work and are co-first authors.



**Citation:** Zeeshan; Ahammad, N.A.; Rasheed, H.U.; El-Deeb, A.A.; Almarri, B.; Shah, N.A. A Numerical Intuition of Activation Energy in Transient Micropolar Nanofluid Flow Configured by an Exponentially Extended Plat Surface with Thermal Radiation Effects. *Mathematics* **2022**, *10*, 4046. <https://doi.org/10.3390/math10214046>

Academic Editors: Juan Francisco Sánchez-Pérez, Gonzalo García Ros and Manuel Conesa

Received: 20 September 2022

Accepted: 27 October 2022

Published: 31 October 2022

**Publisher's Note:** MDPI stays neutral with regard to jurisdictional claims in published maps and institutional affiliations.



**Copyright:** © 2022 by the authors. Licensee MDPI, Basel, Switzerland. This article is an open access article distributed under the terms and conditions of the Creative Commons Attribution (CC BY) license (<https://creativecommons.org/licenses/by/4.0/>).

**Abstract:** In recent times, heat and mass transportation have had some of the most recognized and attractive research areas in computational fluid dynamics. It is useful in the modeling of the flow of nuclear reactors, bioinformatics, the medical discipline, etc. Driven by the execution of the flow in the manufacturing application, the goal of the present analysis is to explore the novel effect of micropolar fluid configured by an exponentially elongated sheet positioned horizontally in a porous channel. The impact of activation energy, internal heating, and heat and mass transfer features are integrated into the revised flow model. A mathematical framework for different flow fields is developed in order to highlight the significant aspects of the thermal and concentration slip effects evaluated on the extended plat surface, with the aid of appropriate transformation factors to diminish the nonlinear fundamental flow equations (PDEs) to a system of (ODEs). Precise numerical treatment for a wide range of pertinent parameters is adopted to solve the nonlinear system through a built-in algorithm in the MATHEMATICA platform. The features of prominent emerging parameters against various flow fields are viewed and addressed through plotted visuals. The influence of the factors on skin friction, heat, and mass coefficients offered through 3D animation is evaluated. The temperature profile improves with ascending values of Brownian parameter and thermophoretic diffusion force but diminishes with subject expansions in Prandtl number and thermal slip parameter. It has been noticed that the concentration outlines increase for reaction rate and activation energy parameters but dwindle for expending values of porosity parameter, Lewis number, and concentration slip parameter. Skin fraction values increase due to the growing nature of the micropolar and second-grade fluid parameters. Nusselt numbers upsurge for increasing thermophoretic diffusion parameters while exhibiting a declining trend for Brownian motion parameters.

**Keywords:** numerical approach; nanofluid; porous media; chemical reaction; extended sheet

**MSC:** 76D05; 76-10

## 1. Introduction

Magnetohydrodynamics is the branch of fluid mechanics that examines the study of electrically conducting liquids with magnetic arenas, such as seawater, electrolytes, or molten metals (MHD). The combined study of fluid dynamics and electromagnetics, sensing, magnetohydrodynamic power production, geophysics, and electromagnetic drug

targeting, and other fields of engineering and sciences, are only a few of the fields in which MHD finds uses. The fascinating books by Roberts [1] and Davidson [2] specifically discuss obvious verifications and a few implementations. Zeeshan et al. [3] and Haroon et al. [4] have conducted a homotopic solution of electrically conductive fluid triggered by an accelerating flat surface beneath the effect of internal heating and chemical reaction. They have specifically carried out research features on motivated magnetics, such as Newtonian heating and reaction rate on unsteady MHD movement through porous media. Whirter et al. [5] studied thermal radiation and MHD flow experimentally through a porous channel. Second-grade channels are a typical subclass of viscoelastic fluid in which the velocity field is a second-order derivative and a second-order tensor. Hakeem et al. [6] have carried out a comparative analysis of non-Newtonian and Newtonian liquids as base fluids across a liquid medium in the presence of a uniform magnetic field. Non-Newtonian fluids are useful in manufacturing on a large scale, which includes, ceramic pastes, inks, petroleum drilling, paints, and much more. Keeping in mind, such crucial importance, several researchers and engineers explored second-grade nanofluid models in different second-grade and boundary postulates. Sarkar et al. [7] and Rasheed et al. [8] studied electrically conductive nanofluid model to analyze the nature of heat and mass transmission in view of a porous channel. Channels et al. [9] and Bilal et al. [10] studied hydromagnetic second-grade fluid through the permeable inclined surface with the impact of internal heating. Moreover, as indicated in [11–18], and other studies therein, nanomaterials have a diversity of dynamic applications in various emerging sciences.

The work required to start the chemical reaction is called activation energy. The entire atoms or nanoparticles in a chemical reaction have either kinetic or potential energy. A Swedish scientist Svabte Arrhenius introduced the idea of the activation energy for the first time. Some of the elements respond to the presence of a fixed energy at the same time.

The impact of the transfer rates of heat and mass in a rotating nanofluid flow subject to Brownian diffusion and chemical reaction effects is offered by Awad et al. [19]. Zaib et al. [20] offered to analyze the radiation effect of stagnation flow of a Carreau fluid configured by a heated flat channel with a Newtonian heating and chemical reaction effect. Majeed et al. [21] surveyed heat transfer mechanisms in electrically conductive fluids with thermal radiation and second-order momentum slip condition effects.

Irfan et al. [22] performed a computation framework for thermally radiative Carreau nanofluid with Arrhenius energy and joule heating effects. Rasheed et al. [23] carried out a computational framework of thermally radiative nanofluid flow driven by a stretching surface. Shah et al. [24] studied the thermally radiative Casson across a nonlinear extended surface with entropy generation. Khan et al. [25] examined micropolar fluid across a permeable rotating disk with micro-organisms and an internal heating effect. Song et al. [26] investigated the impact of radiation in a modified Darcy-law flow model over a rotating stretching disk. Chu et al. [27] inspected the significance of bioconvection and MHD flow in a third-grade fluid model driven by a stretching medium with the Buongiorno flow model. Ramzan et al. [28] explored the role of magnetized 3D ionized nanofluid with a Cattaneo-Christov model, CCM. Waqas et al. [29] inspected the time-dependent flow of nanomaterials configured by a stretching wedge with a melting heat chemical reaction effect. Xia et al. [30] considered convective heat behavior in Eyring fluid flow with bioconvection and microorganisms. Ramesh et al. [31] looked into the bioconvection in Maxwell's nanofluid flow across a Riga plate with radiation effect and activation energy. More information is available in [32–40]. Recently, Riaz et al. [41] investigated the impact carbon nanoparticles in a base fluid with entropy generation. The second-grade fluid containing nanoparticles over the vertical channel studied by Nadeem et al. [42]. Nadeem et al. [43] discussed the Buongiorno-based nanofluid model numerically over a nonlinear stretching sheet.

In the light of the cited literature above, it is praiseworthy to mention that there was an attempt to inspect the heat and mass features of the micropolar fluid flow mechanism on the stretching sheet in view of thermophoretic force, activation energy, and thermal radiation

effects. Therefore, by the massive amount of analysis we interacted with, the phenomenon of thermophoresis diffusion and internal heating are subject to convection boundary layer flow axioms. The resultant boundary layer equations for different flow fields in the form of (PDEs) are diminished to (ODEs) with the aid of transformation variables. The nonlinear flow fields are then engaged numerically through an explicit shooting algorithm via a computational software in the MATHEMATICA 11.0 programming platform.

**2. Flow Configuration and Model**

We consider two-dimensional MHD micropolar fluid with heat and mass transfer transient across a permeable exponentially stretchable plate surface. The influence of solute and energy equations are modified with the impact of activation energy, Brownian movement are incorporated in the proposed model. Additionally, the heat transfer mechanism is estimated by assuming the viscous forces and heat source/sink features are engaged in the revised model. The impact of thermal slip and concentration slip effect is indorsed at the boundary of the stretching surface. The entire flow is triggered by the Lorenz force due to the two magnetic fields in the normal direction and electric field. The stretching velocity is  $u_w$  where the reference velocity is denoted with  $U_0$ , such that  $U_0 > 0$ . Here  $T^*$  and  $C^*$  are the corresponding fluid temperature and concentration,  $T_w^*$  and  $C_w^*$  are the wall temperature and concentration, and away from the wall is indicated by  $T_\infty^*$  and  $C_\infty^*$ . Figure 1 displays the physical sketched of the flow configuration and coordinates under the effect of the applied magnetic field.

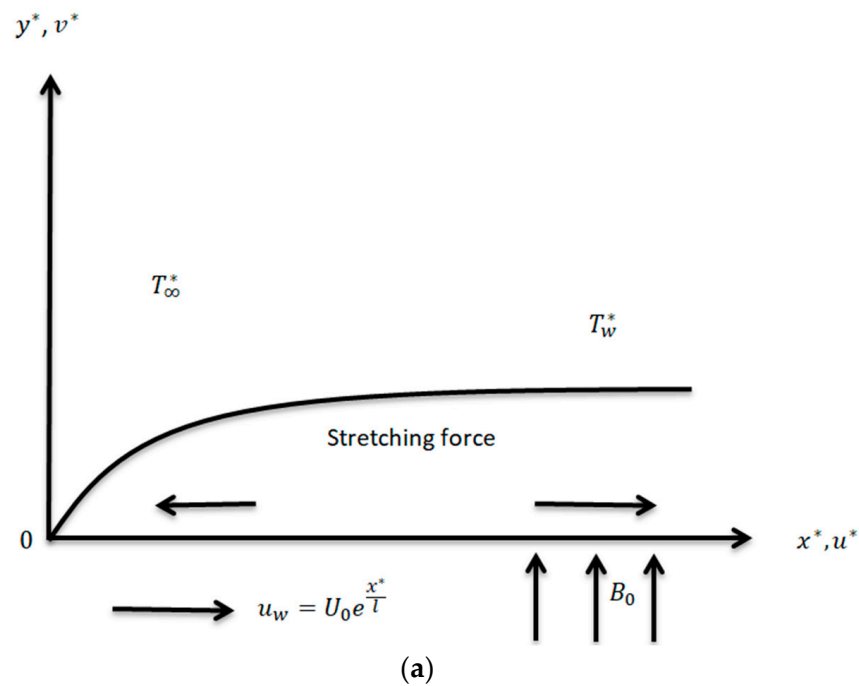


Figure 1. Cont.

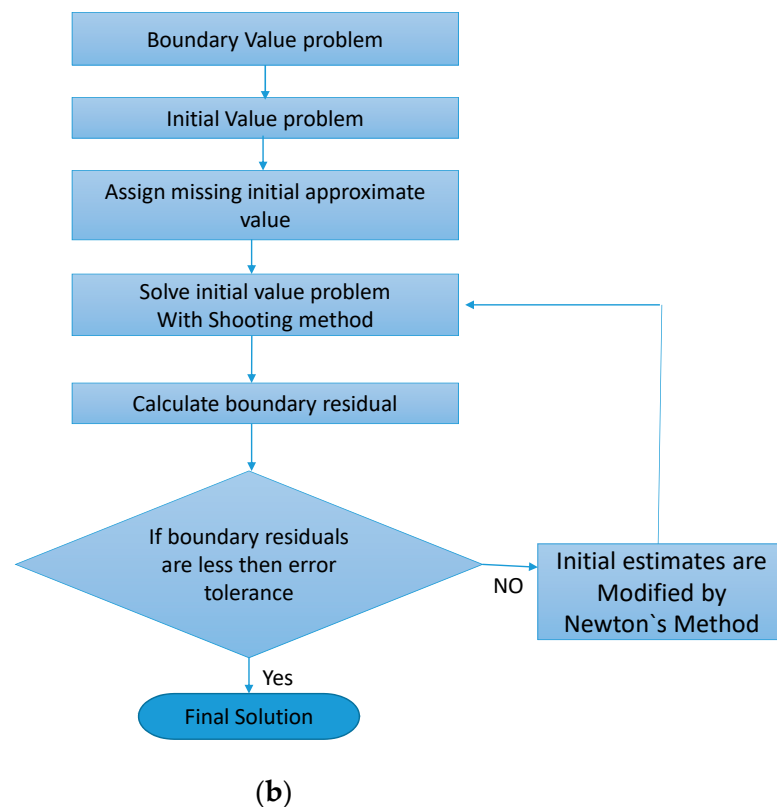


Figure 1. (a) Flow configuration and the coordinates [8]. (b) Flow chart of numerical algorithm [8].

A revised mathematical model is established under the opted assumptions by means of boundary layer approximation in the form of PDES are offered below [37,43]:

$$\frac{\partial u^*}{\partial x^*} + \frac{\partial v^*}{\partial y^*} = 0 \tag{1}$$

$$u^* \frac{\partial u^*}{\partial x^*} + v^* \frac{\partial u^*}{\partial y^*} = \left(\frac{\mu+k_1^*}{\rho}\right) \frac{\partial^2 u^*}{\partial y^{*2}} + \left(\frac{k_1^*}{\rho}\right) \frac{\partial N_1^*}{\partial y^*} + \frac{\alpha_1}{\rho} \left(\frac{\partial}{\partial x^*} \left(u^* \frac{\partial^2 u^*}{\partial y^{*2}}\right) + \frac{\partial u^*}{\partial y^*} \frac{\partial^2 v^*}{\partial y^{*2}} + v^* \frac{\partial^3 v^*}{\partial y^{*3}}\right) - \frac{\sigma B_0^2}{\rho} u^* - \frac{\mu\phi_1}{k_4} u^* \tag{2}$$

$$u^* \frac{\partial N_1^*}{\partial x^*} - v^* \frac{\partial N_1^*}{\partial y^*} = \left(\frac{\gamma^*}{\rho j^*}\right) \frac{\partial^2 N_1^*}{\partial y^{*2}} - \left(\frac{k_1^*}{\rho j^*}\right) \left(2N_1^* + \frac{\partial u^*}{\partial y^*}\right) \tag{3}$$

$$u^* \frac{\partial T^*}{\partial x^*} + v^* \frac{\partial T^*}{\partial y^*} = \alpha \left(\frac{\partial^2 T^*}{\partial y^{*2}}\right) + \tau \left(D_B \frac{\partial C^*}{\partial y^*} \frac{\partial T^*}{\partial y^*} + \frac{D_T^*}{T_\infty^*} \left(\frac{\partial T^*}{\partial y^*}\right)^2\right) + \frac{\alpha_1}{\rho C_p} \frac{\partial u^*}{\partial y^*} \left(\frac{\partial}{\partial y^*} \left(u^* \frac{\partial u^*}{\partial x^*} + v^* \frac{\partial u^*}{\partial y^*}\right)\right) + \left(\frac{\mu+k_1^*}{\rho C_p}\right) \left(\frac{\partial u^*}{\partial y^*}\right)^2 + \frac{q'''}{\rho C_p} \tag{4}$$

$$u^* \frac{\partial C^*}{\partial x^*} + v^* \frac{\partial C^*}{\partial y^*} = D_B \left(\frac{\partial^2 C^*}{\partial y^{*2}}\right) + \frac{D_T}{T_\infty^*} \left(\frac{\partial T^*}{\partial y^*}\right)^2 - Kr^2 \left(\frac{T^*}{T_\infty^*}\right)^m \exp\left(\frac{-Ea}{k_1 T^*}\right) (C^* - C_\infty^*) \tag{5}$$

The heat source/sink term  $q'''$  is exemplified as follows:

$$q''' = \frac{k}{\chi} U_w(x) [A_1(T_w^* - T_\infty^*)F'(\eta) + B_1(T_w^* - T_\infty^*)]$$

Herein,  $A_1$  and  $B_1$  are the temperature and space dependent heat source/sink parameters,  $A_1, B_1 > 0$  signify heat sources whereas  $A_1, B_1 < 0$  are designated for heat sink.

The associative boundary postulates are [43]:

$$\begin{aligned}
 \text{at } y^* = 0 : u^* &= u_w = U_0 e^{\frac{x}{l}}; v^* = 0; N_1^* = -n \frac{\partial u^*}{\partial y^*}; T^* = T_\infty^* + \lambda_1 \frac{\partial T^*}{\partial y^*}; C^* = C_\infty^* + \lambda_2 \frac{\partial C^*}{\partial y^*} \\
 \text{at } y^* = \infty : u^* &= 0; v^* = 0; N_1^* \rightarrow 0; T^* \rightarrow T_\infty^*; C^* \rightarrow C_\infty^*
 \end{aligned}
 \tag{6}$$

whereas  $\rho$  is the fluid density,  $Ea$  is the activation energy coefficient,  $\alpha_1$  is the fluid parameter,  $B_0$  is the external field strength,  $\mu$  is the fluid viscosity,  $\varphi_1$  is the medium of porosity,  $kr$  is the chemical reaction rate,  $k_4$  is the porous medium permeability,  $k_1^*$  is the vortex viscosity,  $\gamma^*$  denotes the spin gradient viscosity,  $C_p$  is the heat capacity,  $j^*$  is the microinertia density,  $\sigma$  is the electrical conductivity,  $D_B$  is the Brownian effect,  $D_{T^*}$  is the thermophoretic effect,  $\tau$  is the heat capacitance ratio,  $U_0$  is the exponential stretching factor,  $\lambda_1$  is the thermal slip coefficient,  $\lambda_2$  is the concentration slip coefficient and  $n$  is the gyration parameter respectively.

Introducing:

$$\begin{aligned}
 \eta &= \left(\frac{U_0}{2lv}\right)^{0.5} \exp\left(\frac{x}{2l}\right)y^*; u^* = U_0 \exp\left(\frac{x}{l}\right)u'_0(\eta); v^* = -\left(\frac{U_0v}{2l}\right)^{0.5} \exp\left(\frac{x}{2l}\right)[u_0(\eta) + \eta u'_0(\eta)]; \\
 N_1^* &= \left(\frac{U_0^3}{2lv}\right)^{0.5} \exp\left(\frac{3x}{2l}\right)h(\eta); T^* = T_\infty^* + T_0^* \exp\left(\frac{x}{2l}\right)\theta(\eta); C^* = C_\infty^* + C_0^* \exp\left(\frac{x}{2l}\right)\varphi(\eta)
 \end{aligned}
 \tag{7}$$

With the assistance of similarity transformation given in Equation (7) the PDEs Equations (2)–(6) are diminished into a dimensionless form given as:

$$(1 + K)u_0'''' + Kh' + u_0u_0'' - 2(u_0')^2 + \beta(5u_0'u_0'''' + 2\eta u_0''u_0'''' + 3u_0''^2 - u_0u_0''''') - 2(\varepsilon + M)u_0' = 0
 \tag{8}$$

$$\left(1 + \frac{K}{2}\right)h'' + u_0h' - 3u_0'h - K(2h + u_0') = 0
 \tag{9}$$

$$\theta'' + \text{Pr} \left[ Nt\theta'^2 - u_0\theta' + 2u_0'\theta + Nb\theta'\varphi' + A_1u_0' + B_1\theta + \beta Ec(u_0'u_0''^2 - u_0u_0''^2 + (1 + K)u_0'^2) \right] = 0
 \tag{10}$$

$$\varphi'' - \text{PrLe}(\varphi u_0' + \varphi' u_0) + 2\varepsilon_1(1 + \varepsilon\theta)^m e^{-\frac{\varepsilon}{(1+\varepsilon\theta)}} \varphi - \frac{Nt}{Nb}\theta'' = 0
 \tag{11}$$

Dimensionless boundary points are:

$$\begin{aligned}
 \text{at } \eta = 0 : u_0 &= 0; u_0' = 1; h = -nu_0''; \theta = 1 + S_1\theta'; \varphi = 1 + S_2\varphi' \\
 \text{at } \eta = \infty : u_0' &\rightarrow 0; h \rightarrow 0; \theta \rightarrow 0; \varphi \rightarrow 0
 \end{aligned}
 \tag{12}$$

The significant physical parameters are symbolized as:

$$\begin{aligned}
 M &= \frac{2\sigma l B_0^2}{\rho U_0}; E = \frac{E_a}{k_1 T_\infty^*}; \text{Pr} = \frac{\mu C_p}{K}; \beta = \frac{U_0 \alpha_1^*}{v \rho l}; Nt = \frac{\tau D_{T^*} \Delta T_0^*}{v T_\infty^*}; \\
 Nb &= \frac{\tau D_B \Delta C}{v T_\infty^*}; \varepsilon = \frac{2lv}{KU_0}; Ec = \frac{u_w^2}{C_p(T_w^* - T_\infty^*)}; Le = \frac{v}{D_B}; K = \frac{k_1}{\mu}; \\
 \varepsilon_1 &= \frac{kr^2}{c}; \varepsilon = \frac{T_w^* - T_\infty^*}{T_\infty^*}; S_1 = \lambda_1 T_0^* \sqrt{\frac{U_0}{2vl}}; S_2 = \lambda_2 C_0^* \sqrt{\frac{U_0}{2vl}}
 \end{aligned}$$

The important physical quantities of interest are characterized as the magnetic field, activation energy, Prandtl number, second-grade fluid parameter, thermophoresis diffusion, Brownian movement, porosity parameter, Eckert and Lewis numbers, micropolar parameter, reaction rate, temperature difference, thermal slip, and concentration slip parameters.

### 3. Parameters of Interest

The significant parameters of interest are the surface force, heat transfer number, and mass flow coefficient, given as follows:

$$Cf_x = \frac{2\tau_w}{\rho u_w^2}, Nu = \frac{xq_w}{k(T^* - T_\infty^*)}, Sh = \frac{xh_m}{k(C^* - C_\infty^*)} \tag{13}$$

$$\tau_w = \frac{\alpha_1}{\rho} \left( u^* \frac{\partial^2 u^*}{\partial y^{*2}} - 2 \frac{\partial u^*}{\partial x^*} \frac{\partial v^*}{\partial y^*} + u^* \frac{\partial^2 u^*}{\partial x^* \partial y^*} + \left( \frac{\mu + k_1^*}{\rho} \right) \frac{\partial u^*}{\partial y^*} + k_1^* N_1^* \right) \Big|_{y^*=0} \tag{14}$$

$$q_w = - \frac{\partial T^*}{\partial y^*} k \Big|_{y^*=0} \tag{15}$$

$$q_m = - \frac{x}{(C_w^* - C_\infty^*)} \frac{\partial C^*}{\partial y^*} \Big|_{y^*=0} \tag{16}$$

The dimensionless form of the parameters of interest are  $Cf$ ,  $Nu$ , and  $Sh$  and are signified as:

$$Cf = [3\beta u_0' u_0'' - \beta u_0 u_0''' + (1 + K)u_0''] \left( \frac{Re_x}{2} \right)^{-0.5} \Big|_{\eta=0} \tag{17}$$

$$\frac{1}{\sqrt{Re_x}} \sqrt{\frac{2l}{x}} Nu = -\theta'(0) \tag{18}$$

$$\frac{1}{\sqrt{Re_x}} \sqrt{\frac{2l}{x}} Sh = -\varphi'(0) \tag{19}$$

whereas  $q_m$  signifies heat flux;  $h_m$  denotes mass flux;  $\tau_w$  is the wall shear stress; and  $Re_x$  is the Reynolds number.

### 4. Numerical Solution

In this section, the nonlinear ordinary differential Equations (8)–(11) subjected to extremes conditions in Equation (13) computed numerically by using RK4 along with the shooting technique are discussed. A detailed procedure can be found in [43]. The resulting equations are diminished into a system of first order differential equations through suitable transformation techniques. The system of first order equations is then integrated numerically via the Runge-Kutta (RK-4) method with an appropriate choice of  $u_0'''(0)$ ,  $h'(0)$ ,  $\theta'(0)$  and  $\varphi'(0)$ . Newton’s method is then used to iteratively estimate the values of  $u_0'''(0)$ ,  $h'(0)$ ,  $\theta'(0)$  and  $\varphi'(0)$ , such that solutions approach zero with the desired accuracy of  $10^{-6}$ .

In addition to studying and facilitating learning the shooting technique algorithm manner, a flow chart is labeled in Figure 1b.

### 5. Discussion

In a prevailing effort, the two-dimensional micropolar fluid flow in view of the external magnetic source subject to and slip boundary postulates driven by an extended exponentially permeable stretchable surface are evaluated. The approximate numerical computations are apprehended through the manifold governing parameters. The consequences pertinent field and the physical conditions of the flow problem are examined by visualizing the impact of manifold parameters. For computational analysis, the successive values of the default flow parameters are deputized as:  $\beta = 0.5$ ,  $K = 0.4$ ,  $M = 0.30$ ,  $\epsilon = 0.1$ ,  $n = 0.3$ ,  $Ec = 0.5$ ,  $Nb = 0.5$ ,  $Nt = 0.5$ ,  $Pr = 0.06$ ,  $Le = 0.4$ ,  $Kr = 0.50$ ,  $S_1 = 0.5$ ,  $S_2 = 0.5$ . The graphical behaviors of the upstairs flow terms on the velocity profile, micropolar distribution, energy field, concentration distribution, drag force coefficient, heat transfer, and mass flow coefficient are scrutinized in Figures 2–26.

Figure 2 reveals the effect of  $\beta$  on velocity outlines  $u'_0(\eta)$ . From this graph, it is witnessed that as expanding behavior  $\beta$  upsurges, the velocity field curves increase. In reality, the momentum diffusivity enhances through higher estimation of the  $\beta$  parameter. As expected,  $u'_0(\eta)$  increases. Figure 3 explains the consequence of the micropolar parameter  $K$  on  $u'_0(\eta)$  field. As shown, the expanding values of  $K$  increases the fluid flow significantly in the boundary region. Physically, larger expansion of micropolar parameter enhances fluid movement. Consequently,  $u'_0(\eta)$  profile increases. Figure 4 demonstrates the influences of  $M$  on  $u'_0(\eta)$  field. From this visual it is perceived that  $u'_0(\eta)$  diminishes through a higher estimation magnetic parameter. Actually, increasing the values of  $M$  develops the resistive force of fluid flow and the associative layer thickness due to the Lorenz force. Thus, velocity and associative boundary layer thickness declines. Figure 5 elaborates the porous medium parameter  $\varepsilon$  impact on  $u'_0(\eta)$ . Evidently an augmentation in the  $\varepsilon$  magnitude diminishes fluid flow. Consequently, larger  $\varepsilon$  estimations create a decline in  $u'_0(\eta)$  and related layer thickness. The outcome of  $K$  on micropolar distribution  $g(\eta)$  is addressed via Figure 6. This figure illustrates the enhancement in  $h(\eta)$  subject to an increment in micropolar parameter  $K$ . Thus,  $h(\eta)$  enhances. The influence of  $n$  is interpreted in Figure 7. Clearly  $h(\eta)$  enhances with higher values of constant  $n$ . Variations of Eckert number  $Ec$  for scrutinization of energy field  $\theta(\eta)$  are disclosed in Figure 8. Larger  $Ec$  corresponds to an enhancement  $\theta(\eta)$  in the flow region. Physically, such scenario is observed because kinetic energy (K.E) of the fluid particles increases with the expanding values of  $Ec$  and ultimate  $\theta(\eta)$  boosts. Figure 9 elaborates on  $Nb$  impression on  $\theta(\eta)$ . Evidently an expansion in the  $Nb$  upsurges the speed through which fluid particles move faster in arbitrary direction with diverse random path owing to the Brownian aspect. Consequently, stronger estimations of  $Nb$  enhance energy profile and related thermal boundary layer thickness. Figure 10 reveals  $Nt$  variations subject to  $\theta(\eta)$ . Here,  $\theta(\eta)$  expands through higher  $Nt$ . Actually, thermophoresis diffusion increases when diffusion coefficient  $Nt$  is increased. Such force assists to outflow nanoscale particles by a region towards colder region and eventual  $T(\eta)$  lifts. Effect of  $Pr$  on energy profile  $\theta(\eta)$  is revealed in Figure 11. Here,  $\theta(\eta)$  reduces with expanding values of  $Pr$  estimations. It is clear from this visual that variations in  $Pr$  is why the thermal nature of the nanofluid diminishes that indicates a dwindle in the internal heating. Subsequently, boundary layers' thickness and the energy field of the nanofluid dwindle in the flow domain. The result of the slip parameter  $S_1$  on  $\theta(\eta)$  is attained via Figure 12. This plot exemplifies declines in  $\theta(\eta)$ . In fact, the thermal layer and energy distribution enhances with higher values of slip parameter. Thus  $\theta(\eta)$  decreases. Attributes of  $\beta$  are outlined in Figure 13. Here, the thermal energy found lower  $\theta(\eta)$  subject to increment in the second-grade fluid parameter. Such situation is noticed due to higher values of  $\beta$  implies destruction in thermal boundary layer density effectively. In consequence,  $\theta(\eta)$  diminishes. The contribution of the space dependent heat generation/sinks parameter  $A_1$  on  $\theta(\eta)$  is estimated through Figure 14. One can identify that  $\theta(\eta)$  diminishes through higher estimation of  $A_1$  and related boundary layer. Figure 15 depicts  $\theta(\eta)$  variations subjected to  $B_1$ . This plot reveals that  $\theta(\eta)$  dwindles at a stronger different dependent parameter  $B_1$ . Physically, the working fluid lost energy for expanding values of  $B_1$ . In consequence  $\theta(\eta)$  declines.

The concentration field  $\varphi(\eta)$  curves for reaction rate parameter  $\varepsilon_1$  are revealed in Figure 16. One can recognize that  $\varphi(\eta)$  is an increasing function of  $\varepsilon_1$ . Physically, higher estimation of  $\varepsilon_1$  leads to activation energy on the  $\varphi(\eta)$ . Attributes of energy parameter  $E$  on  $\varphi(\eta)$  is elaborated in Figure 17. This figure confirms that  $\varphi(\eta)$  upsurges subject to increases in  $E$  of the nanofluid. Figure 18 explains the Lewis number  $Le$  effects on  $\varphi(\eta)$ . As anticipated as  $\varphi(\eta)$  increases so does  $Le$ , which leads to upshots in the mass flow rate considerably. Similarly, the  $\varphi(\eta)$  rate at sheet surface improves. Additionally,  $\varphi(\eta)$  of the nanofluid to the sheet surface decays with larger values of  $Le$ . The contribution of concentration slip  $S_2$  against concentration profile  $\varphi(\eta)$  is estimated through Figure 19. As noticed from this plot, growing values of  $S_2$  diminishes the concentration distribution.

Hence,  $\varphi(\eta)$  decays. The implication of  $\varepsilon$  on  $\varphi(\eta)$  is publicized in Figure 20. One can recognize from this visual that  $\varphi(\eta)$  decreases the function of temperature ratio parameter.

Figures 21–26 show the attribute of different pertinent parameters on surface force coefficient  $Cf_x$ , heat transfer  $Nu_x$ , and mass flow rate  $Sh_x$  coefficients. It can be concluded from Figures 21 and 22 that the drag force increases at higher estimations of  $M$ ,  $K$  and  $\beta$ . Figures 23 and 24 display a lower heat transfer  $Nu_x$  due to the  $Pr$ ,  $Ec$ ,  $Nb$  and  $Nt$  parameters. Figures 25 and 26 portray mass flow rate  $Sh_x$  for numerous estimates of  $Pr$ ,  $Le$ ,  $Nb$  and  $Nt$ . The mass flow develops in the case of larger estimation of the proposed  $Pr$  and  $Le$  parameters, while it diminishes as the values of  $Nb$  and  $Nt$  increase.

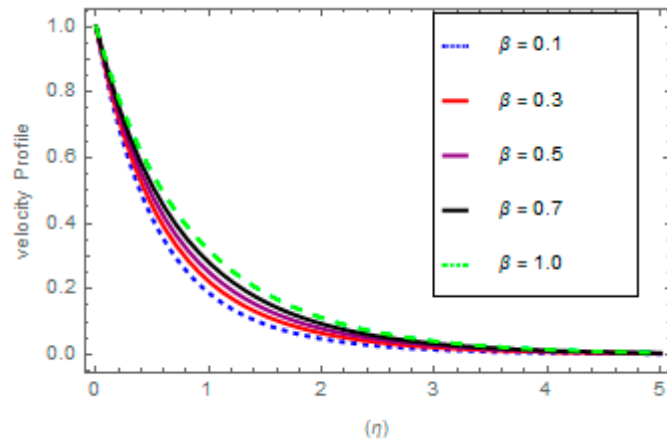


Figure 2. Upshot of  $\beta$  on  $u'_0(\eta)$ .

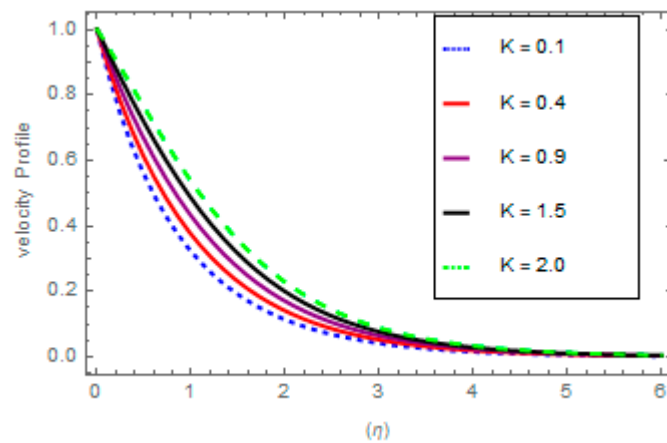


Figure 3. Upshot of  $K$  on  $u'_0(\eta)$ .

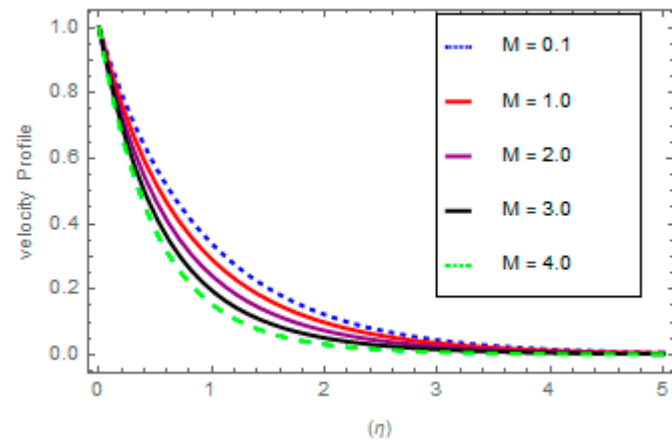


Figure 4. Upshot of M on  $u'_0(\eta)$ .

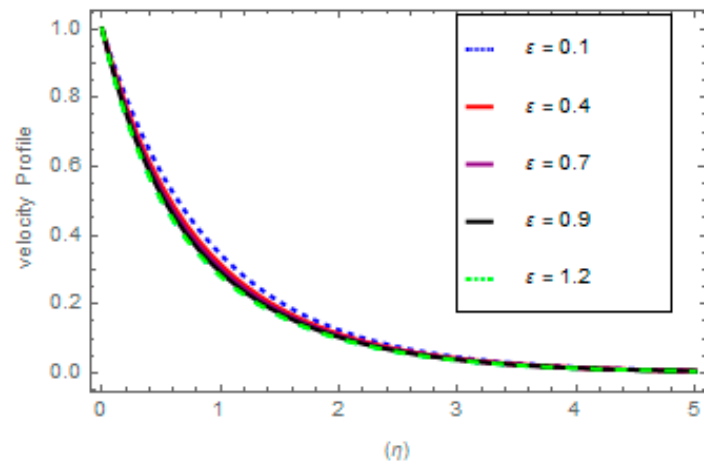


Figure 5. Upshot of  $\epsilon$  on  $u'_0(\eta)$ .

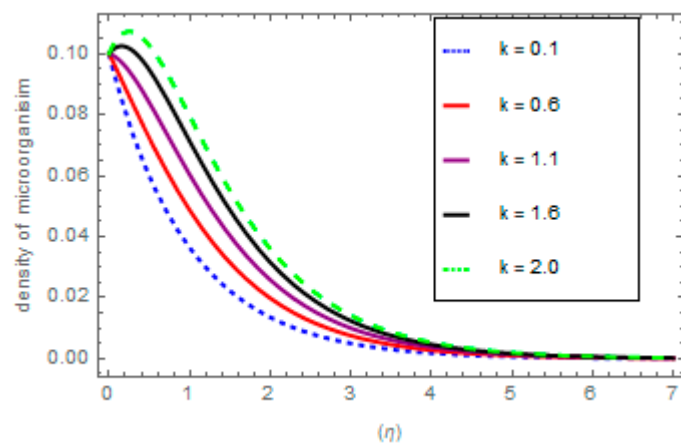


Figure 6. Upshot of K on  $h(\eta)$ .

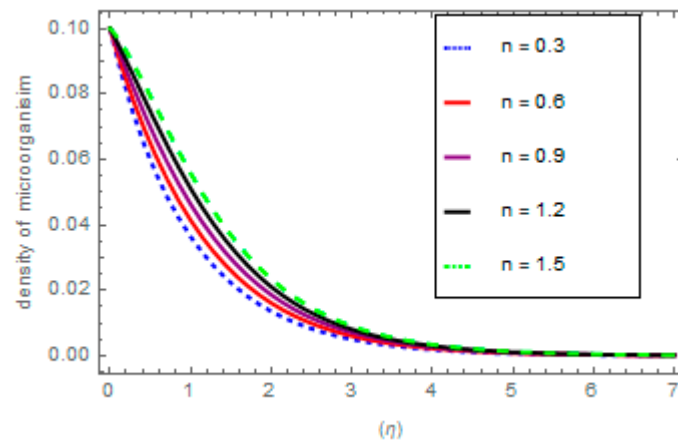


Figure 7. Upshot of  $n$  on  $h(\eta)$ .

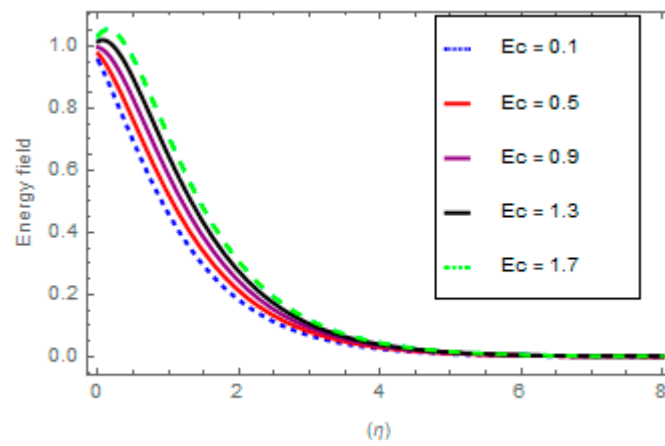


Figure 8. Result of  $E_c$  via  $\theta(\eta)$ .

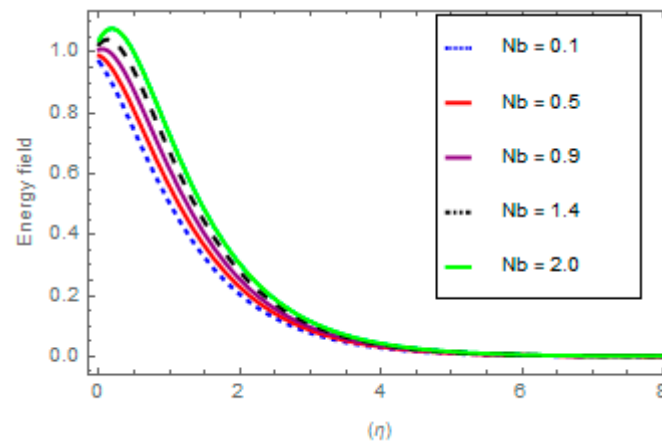


Figure 9. Result of  $N_b$  via  $\theta(\eta)$ .

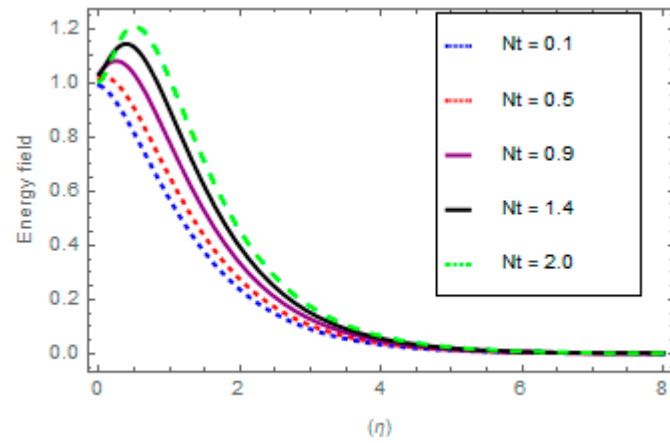


Figure 10. Result of  $Nt$  via  $\theta(\eta)$ .

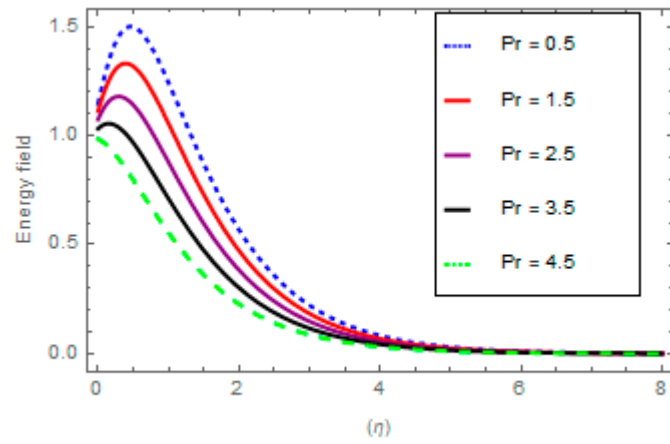


Figure 11. Result of  $Pr$  via  $\theta(\eta)$ .

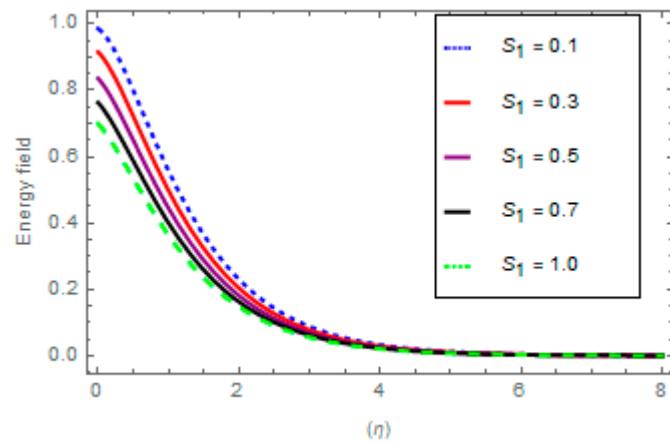


Figure 12. Result of  $S_1$  via  $\theta(\eta)$ .

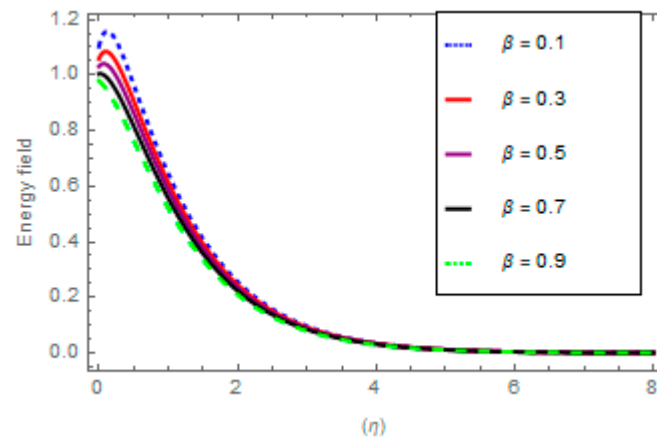


Figure 13. Result of  $\beta$  via  $\theta(\eta)$ .

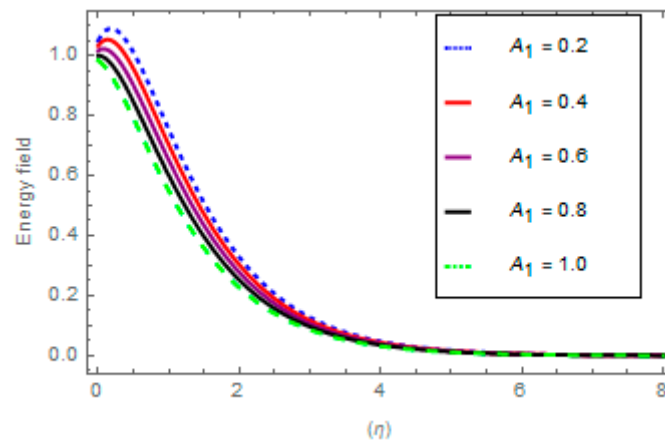


Figure 14. Result of  $A_1$  via  $\theta(\eta)$ .

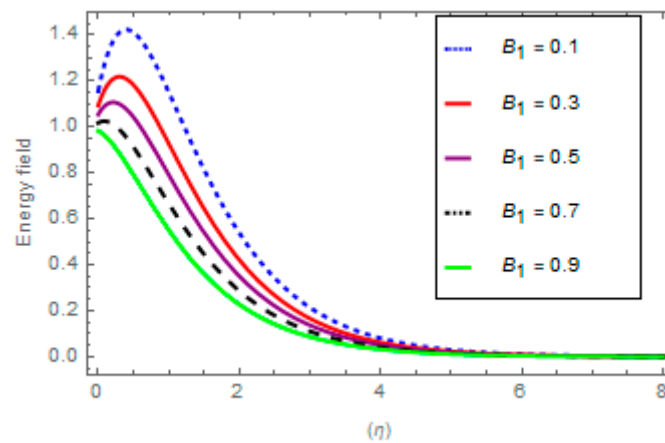


Figure 15. Result of  $B_1$  via  $\theta(\eta)$ .

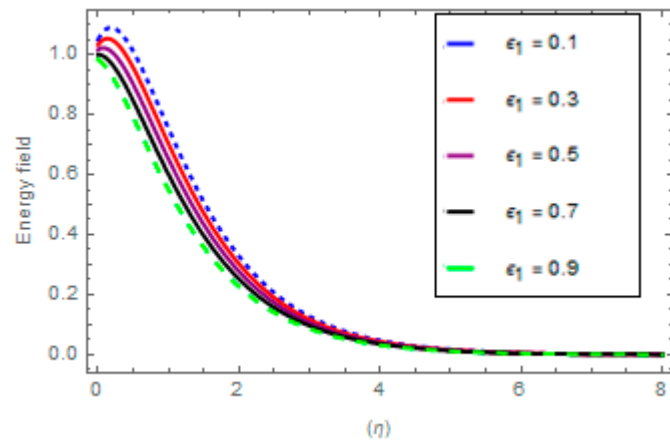


Figure 16. Result of  $\epsilon_1$  via  $\varphi(\eta)$ .

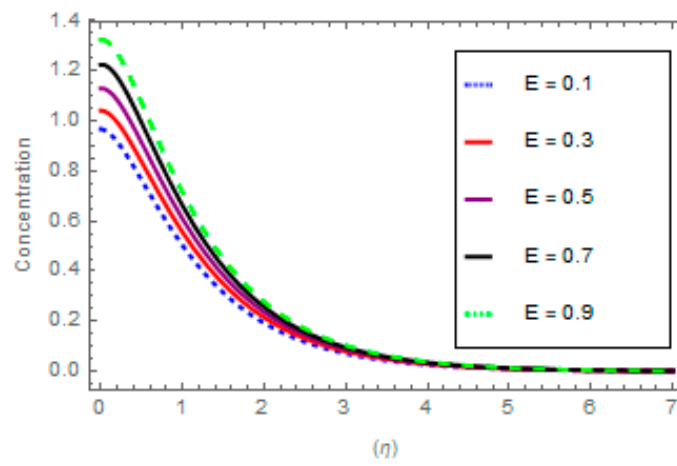


Figure 17. Result of  $E$  via  $\varphi(\eta)$ .

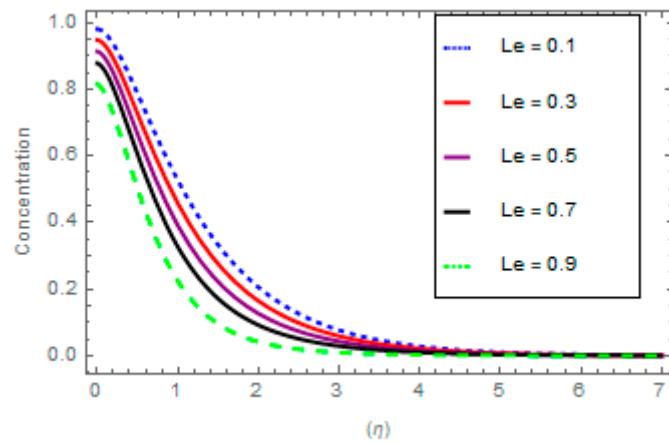


Figure 18. Result of  $Le$  via  $\varphi(\eta)$ .

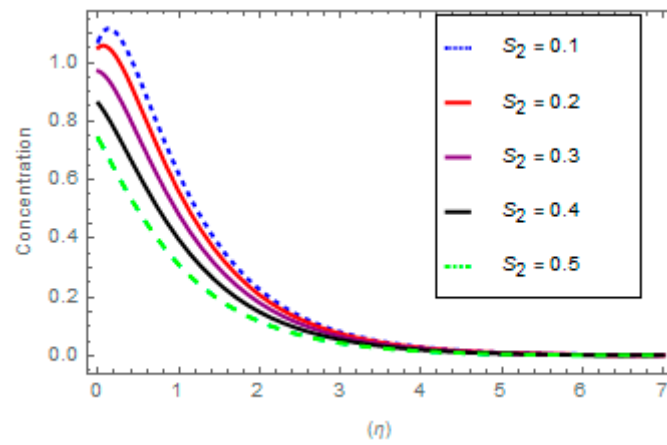


Figure 19. Result of  $S_2$  via  $\varphi(\eta)$ .

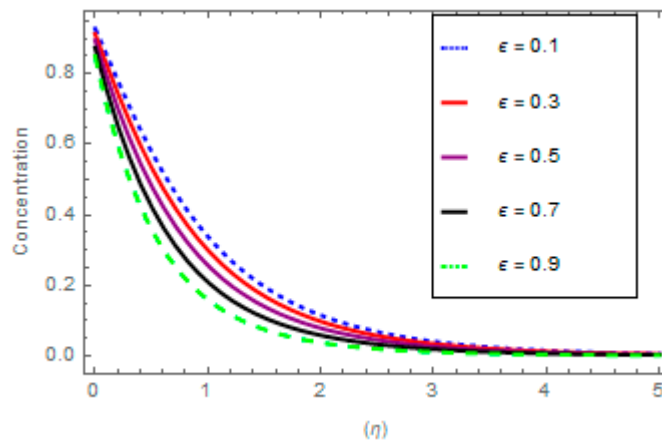


Figure 20. Result of  $\epsilon$  via  $\varphi(\eta)$ .

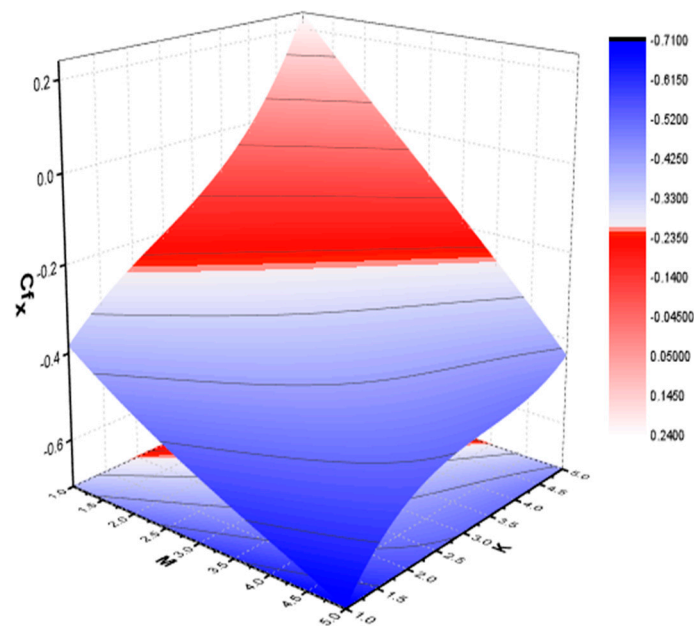


Figure 21. 3D visual of  $Cf_x$  for  $M$  and  $K$ .

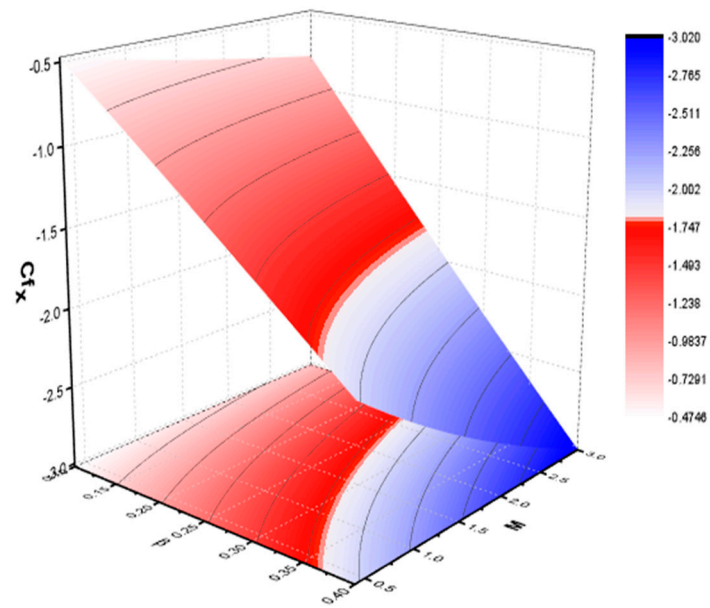


Figure 22. 3D visual of  $Cf_x$  for  $\beta$  and  $M$ .

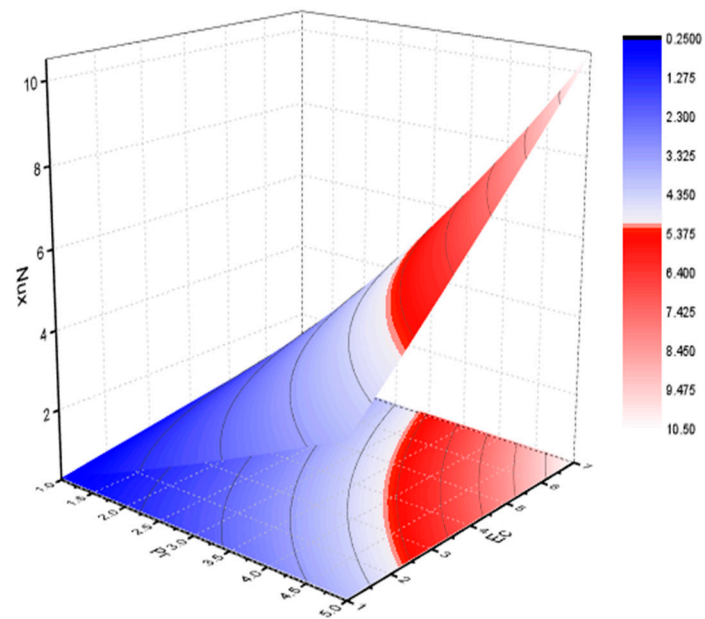


Figure 23. 3D visual of  $Nu_x$  for  $Pr$  and  $Ec$ .

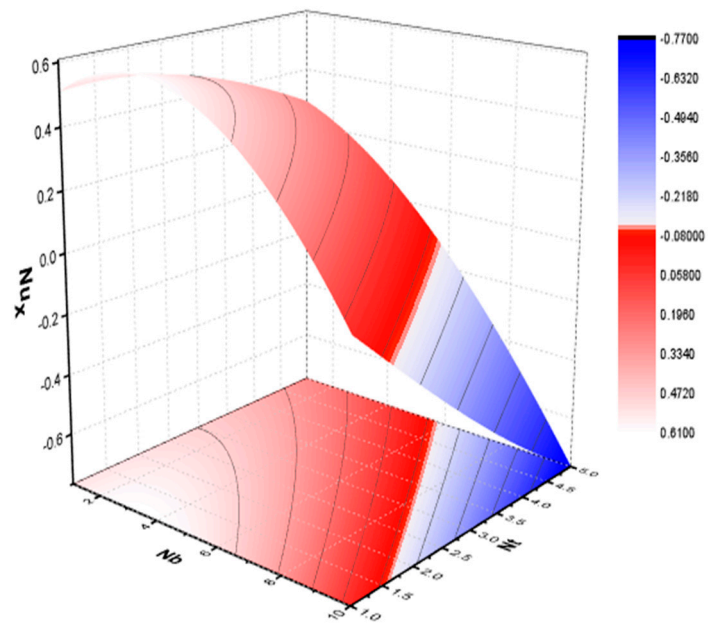


Figure 24. 3D visual of  $Nu_x$  for  $Nb$  and  $Nt$ .

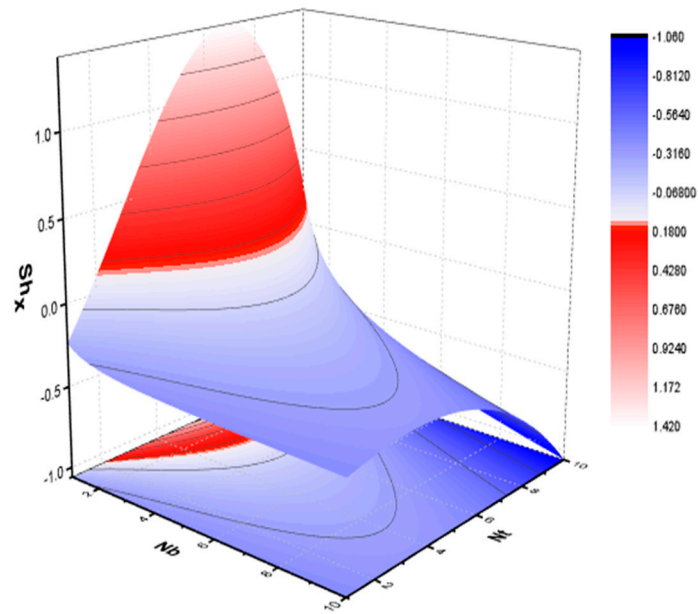


Figure 25. 3D visual of  $Sh_x$  for  $Nb$  and  $Nt$ .

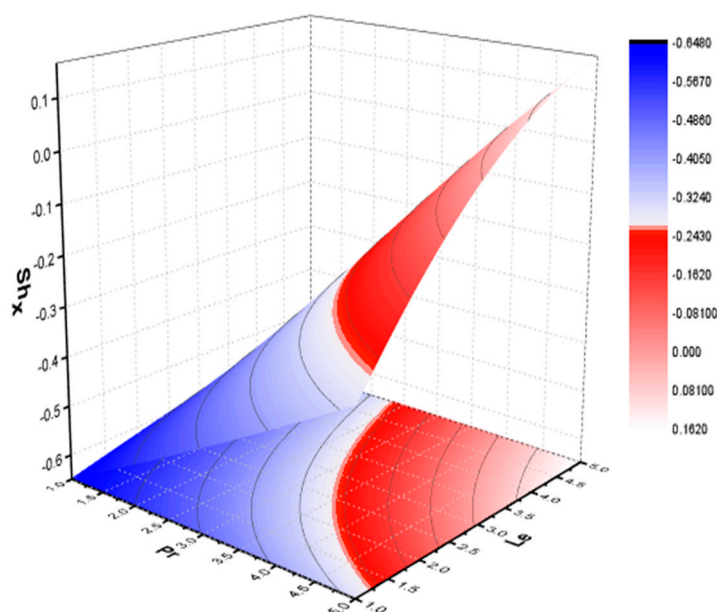


Figure 26. 3D visual of  $Sh_x$  for Pr and Le.

## 6. Conclusions

Computational modeling for two-dimensional MHD micropolar flow with nanoparticles towards an exponentially extended surface with nonlinear heat source parameter and reaction parameter is evaluated. The resulting dimensionless nonlinear framework of (ODEs) is solved through built-in algorithms running the numerical code in the MATHEMATICA 11.0 platform. The specific outcomes are shown after conducting the complete study and are summarized below:

- Velocity outlines increase with the growth of the fluid parameter due to the resistive force, while velocity outlines fall with the increasing values of porosity parameters.
- It is observed that the linear and angular velocity outlines increase subject to variations in the values of micropolar parameters.
- The temperature profile improves with ascending values of Brownian parameter and thermophoretic diffusion force but diminishes with the increasing values of Prandtl number and thermal slip parameters.
- It has been noticed that the concentration outlines incremented for reaction rate and activation energy parameters but dwindled for expending values of porosity parameters, the Lewis number, and concentration slip parameters.
- Skin fraction values increase because of the growing nature of the micropolar factor.
- Nusselt number upsurges for increasing thermophoretic diffusion parameter while exhibits declining trend for Brownian motion parameter.
- The mass diffusion rate improves when subjected to higher values of Prandtl and Lewis numbers. On the contrary, it decreases with Brownian and thermophoresis diffusion force.

**Author Contributions:** Data curation, Z. and N.A.S.; Methodology, N.A.A.; Software, H.U.R.; Visualization, A.A.E.-D.; Writing—original draft, Z. and N.A.S.; Writing—review & editing, B.A. All authors have read and agreed to the published version of the manuscript.

**Funding:** This research was funded by Princess Nourah bint Abdulrahman University Researchers Supporting Project number (PNURSP2022R216), Princess Nourah bint Abdulrahman University, Riyadh, Saudi Arabia.

**Institutional Review Board Statement:** Not applicable.

**Informed Consent Statement:** Not applicable.

**Data Availability Statement:** Not applicable.

**Conflicts of Interest:** The authors declare no conflict of interest.

## Nomenclature

$(u^*, v^*)$	Velocity components along $x^*$ and $y^*$ axes	$N_1^*$	Motile microorganism component
$\mu$	Kinematics viscosity	$\alpha_1$	Material parameter of the fluid
$k_1^*$	Coefficient of viscosity	$\sigma$	Fluid conductivity
$\rho$	Density parameter	$B_0$	Magnetic field
$\varphi_1$	Porous medium	$\tau$	Ratio of heat capacitance
$K$	Permeability of the medium	$D_B$	Brownian diffusion
$\gamma$	Spin gradient	$T^*$	Fluid temperature
$j^*$	Micro inertia	$T_\infty^*$	Free stream temperature
$D_{T^*}$	Thermophoretic coefficient	$C^*$	Concentration component
$c_p$	Specific heat	$C_\infty^*$	Ambient concentration
$Kr$	Chemical reaction rate	$n$	Constant
$u_w$	Stretching velocity of the sheet	$Ea$	Activation energy coefficient
$\lambda_1$	Thermal slip factor	$U_0$	Exponential stretching coefficient
$\lambda_2$	Concentration slip coefficient	$k$	Microgyration Parameter
$T^*$	Fluid parameter	$M$	Magnetic field
$K$	Porous medium	$Pr$	Prandtl Number
$F'$	Dimensionless velocity	$T$	Dimensionless temperature
$g$	Dimensionless motile microorganism	$Nb$	Brownian motion
$C$	Dimensionless concentration	$Nt$	Thermophoresis parameter
$Le$	Lewis number	$\varepsilon_1$	Reaction rate
$S_1$	Thermal slip parameter	$\varepsilon$	Temperature ratio
$S_2$	Concentration slip parameter	$E$	Parameter of Activation energy
$Cf_x$	Skin friction	$Nu_x$	Nusselt number
$Re_x$	Reynolds Number	$Sh_x$	Sherwood number

## References

- Roberts, P.H. *An Introduction to Magnetohydrodynamics*; Longmans: London, UK, 1967.
- Davidson, P.A. *An Introduction to Magnetohydrodynamics*; American Association of Physics Teachers: College Park, MD, USA, 2002.
- Zeeshan, K.; Rasheed, H.U.; Khan, I.; Abu-Zinadah, H.; Aldahlan, M.A. Mathematical Simulation of Casson MHD Flow through a Permeable Moving Wedge with Nonlinear Chemical Reaction and Nonlinear Thermal Radiation. *Materials* **2022**, *15*, 747. [[CrossRef](#)]
- Rasheed, H.U.; Khan, Z.; El-Zahar, E.R.; Shah, N.A.; Islam, S.; Abbas, T. Homotopic solutions of an unsteady magnetohydrodynamic flow of Casson nanofluid flow by a vertical cylinder with Brownian and viscous dissipation effects. *Waves Random Complex Media* **2022**. [[CrossRef](#)]
- McWhirter, J.D.; Crawford, M.E.; Klein, D.E. Magnetohydrodynamic flows in porous media II: Experimental results. *Fusion Technol.* **1998**, *34*, 187–197. [[CrossRef](#)]
- Hakeem, A.A.; Saranya, S.; Ganga, B. Comparative study on Newtonian/non-Newtonian base fluids with magnetic/non-magnetic nanoparticles over a flat plate with uniform heat flux. *J. Mol. Liq.* **2017**, *230*, 445–452. [[CrossRef](#)]
- Sarkar, S.; Endalew, M.F.; Makinde, O.D. Study of MHD Second Grade Flow through a Porous Microchannel under the Dual-Phase-Lag Heat and Mass Transfer Model. *J. Appl. Comput. Mech.* **2019**, *5*, 763–778.
- Rasheed, H.U.; Islam, S.; Zeeshan; Khan, J.; Abbas, T.; Mohmand, M.I. Numerical solution of chemically reactive and thermally radiative MHD Prandtl nanofluid over a curved surface with convective boundary conditions. *ZAMM-J. Appl. Math. Mech.* **2021**, e202100125. [[CrossRef](#)]
- Rasheed, H.U.; Islam, S.; Zeeshan; Abbas, T.; Khan, J. Analytical treatment of MHD flow and chemically reactive Casson fluid with Joule heating and variable viscosity effect. *Waves Random Complex Media* **2022**. [[CrossRef](#)]
- Awan, A.B.; Zubair, M.; Memon, Z.A.; Ghalleb, N.; Tlili, I. Comparative analysis of dish Stirling engine and photovoltaic technologies: Energy and economic perspective. *Sustain. Energy Technol. Assess.* **2021**, *44*, 101028. [[CrossRef](#)]
- Raza, Q.; Qureshi, M.Z.A.; Khan, B.A.; Kadhim Hussein, A.; Ali, B.; Chung, J.D. Insight into dynamic of mono and hybrid nanofluids subject to binary chemical reaction, activation energy, and magnetic field through the porous surfaces. *Mathematics* **2022**, *10*, 3013. [[CrossRef](#)]
- Veeram, G.; Poojitha, P.; Katta, H.; Hemalatha, S.; Babu, M.J.; Raju, C.S.K.; Yook, S.-J. Simulation of dissipative hybrid nanofluid (PEG-Water + ZrO<sub>2</sub> + MgO) flow by a curved shrinking sheet with thermal radiation and higher order chemical reaction. *Mathematics* **2022**, *10*, 1706. [[CrossRef](#)]

13. Rasheed, H.U.; Zeeshan. Homotopic framework for the Buongiorno model of 2D viscoelastic nanofluid flow toward a porous curve surface with ohmic heating and Brownian diffusion effects. *Waves Random Complex Media* **2022**. [[CrossRef](#)]
14. Lou, Q.; Ali, B.; Rehman, S.U.; Habib, D.; Abdal, S.; Chung, J.D. Micropolar dusty fluid: Coriolis force effects on dynamics of MHD rotating fluid when Lorentz force is significant. *Mathematics* **2022**, *10*, 2630. [[CrossRef](#)]
15. Ashraf, M.Z.; Rehman, S.U.; Farid, S.; Hussein, A.K.; Ali, B.; Weera, W. Insight into significance of bioconvection on MHD tangent hyperbolic nanofluid flow of irregular thickness across a slender elastic surface. *Mathematics* **2022**, *10*, 2592. [[CrossRef](#)]
16. Ur Rasheed, H.; AL-Zubaidi, A.; Islam, S.; Saleem, S.; Khan, Z.; Khan, W. Effects of Joule Heating and Viscous Dissipation on Magnetohydrodynamic Boundary Layer Flow of Jeffrey Nanofluid over a Vertically Stretching Cylinder. *Coatings* **2021**, *11*, 353. [[CrossRef](#)]
17. Shah, N.A.; Wakif, A.; El-Zahar, E.R.; Ahmad, S.; Yook, S.-J. Numerical simulation of a thermally enhanced EMHD flow of a heterogeneous micropolar mixture comprising (60%)-ethylene glycol (EG), (40%)-water (W), and copper oxide nanomaterials (CuO). *Case Stud. Therm. Eng.* **2022**, *35*, 102046. [[CrossRef](#)]
18. Sajjan, K.; Ahammad, N.A.; Raju, C.S.K.; Kumar, M.D.; Weera, W. Nonlinear Boussinesq and Rosseland approximations on 3D flow in an interruption of Ternary nanoparticles with various shapes of densities and conductivity properties. *AIMS Math.* **2022**, *7*, 18416–18449. [[CrossRef](#)]
19. Majeed, A.; Noori, F.M.; Zeeshan, A.; Mahmood, T.; Rehman, S.U.; Khan, I. Analysis of activation energy in magnetohydrodynamic flow with chemical reaction and second order momentum slip model. *Case Stud. Therm. Eng.* **2018**, *12*, 765–773. [[CrossRef](#)]
20. Irfan, M.; Khan, M.; Khan, W.A.; Ahmad, L. Influence of binary chemical reaction with Arrhenius activation energy in MHD nonlinear radiative flow of unsteady Carreau nanofluid: Dual solutions. *Appl. Phys. A* **2019**, *125*, 179. [[CrossRef](#)]
21. Rasheed, H.U.; Islam, S.; Khan, Z.; Alharbi, S.O.; Khan, W.A.; Khan, W.; Khan, I. Thermal Radiation Effects on Unsteady Stagnation Point Nanofluid Flow in View of Convective Boundary Conditions. *Math. Probl. Eng.* **2021**, *2021*, 5557708. [[CrossRef](#)]
22. Shah, Z.; Kumam, P.; Deebani, W. Radiative MHD Casson nanofluid flow with activation energy and chemical reaction over past nonlinearly stretching surface through entropy generation. *Sci. Rep.* **2020**, *10*, 4402. [[CrossRef](#)]
23. Khan, M.I.; Waqas, H.; Khan, S.U.; Imran, M.; Chu, Y.M.; Abbasi, A.; Kadry, S. Slip flow of micropolar nanofluid over a porous rotating disk with motile microorganisms, nonlinear thermal radiation and activation energy. *Int. Commun. Heat Mass Transf.* **2021**, *122*, 105161. [[CrossRef](#)]
24. Song, Y.Q.; Khan, S.A.; Imran, M.; Waqas, H.; Khan, S.U.; Khan, M.I.; Qayyum, S.; Chu, Y.M. Applications of modified Darcy law and nonlinear thermal radiation in bioconvection flow of micropolar nanofluid over an off centered rotating disk. *Alex. Eng. J.* **2021**, *60*, 4607–4618. [[CrossRef](#)]
25. Chu, Y.M.; Khan, M.I.; Khan, N.B.; Kadry, S.; Khan, S.U.; Tlili, I.; Nayak, M.K. Significance of activation energy, bio-convection and magnetohydrodynamic in flow of third grade fluid (non-Newtonian) towards stretched surface: A Buongiorno model analysis. *Int. Commun. Heat Mass Transf.* **2020**, *118*, 104893. [[CrossRef](#)]
26. Ramzan, M.; Gul, H.; Kadry, S.; Chu, Y.M. Role of bioconvection in a three dimensional tangent hyperbolic partially ionized magnetized nanofluid flow with Cattaneo-Christov heat flux and activation energy. *Int. Commun. Heat Mass Transf.* **2021**, *120*, 104994. [[CrossRef](#)]
27. Waqas, H.; Khan, S.A.; Khan, S.U.; Khan, M.I.; Kadry, S.; Chu, Y.M. Falkner-Skan time-dependent bioconvection flow of cross nanofluid with nonlinear thermal radiation, activation energy and melting process. *Int. Commun. Heat Mass Transf.* **2021**, *120*, 105028. [[CrossRef](#)]
28. Xia, W.F.; Haq, F.; Saleem, M.; Ijaz Khan, M.; Khan, S.U.; Chu, Y.M. Irreversibility analysis in natural bio-convective flow of Eyring-Powell nanofluid subject to activation energy and gyrotactic microorganisms. *Ain Shams Eng. J.* **2021**, *12*, 4063–4074. [[CrossRef](#)]
29. Ramesh, K.; Khan, S.U.; Jameel, M.; Khan, M.I.; Chu, Y.M.; Kadry, S. Bioconvection assessment in Maxwell nanofluid configured by a Riga surface with nonlinear thermal radiation and activation energy. *Surf. Interfaces* **2020**, *21*, 100749. [[CrossRef](#)]
30. Waqas, M.; Jabeen, S.; Hayat, T.; Shehzad, S.A.; Alsaedi, A. Numerical simulation for nonlinear radiated Eyring-Powell nanofluid considering magnetic dipole and activation energy. *Int. Commun. Heat Mass Transf.* **2020**, *112*, 104401. [[CrossRef](#)]
31. Sandhya, G.; Sarojamma, G.; Satya Narayana, P.V.; Venkateswarlu, B. Buoyancy forces and activation energy on the MHD radiative flow over an exponentially stretching sheet with second-order slip. *Heat Transf.* **2021**, *50*, 784–800. [[CrossRef](#)]
32. Irfan, M.; Rafiq, K.; Khan, M.; Waqas, M.; Anwar, M.S. Theoretical analysis of new mass flux theory and Arrhenius activation energy in Carreau nanofluid with magnetic influence. *Int. Commun. Heat Mass Transf.* **2021**, *120*, 105051. [[CrossRef](#)]
33. Khan, M.I.; Alzahrani, F. Nonlinear dissipative slip flow of Jeffrey nanomaterial towards a curved surface with entropy generation and activation energy. *Math. Comput. Simul.* **2021**, *185*, 47–61. [[CrossRef](#)]
34. Rasheed, H.U.; Khan, W.; Khan, I.; Alshammari, N.; Hamadneh, N. Numerical computation of 3D Brownian motion of thin film nanofluid flow of convective heat transfer over a stretchable rotating surface. *Sci. Rep.* **2022**, *12*, 2708. [[CrossRef](#)]
35. Koriko, O.K.; Saleem, S.; Chung, J.D.; Omowaye, A.J.; Oreyni, T. Exploration of bioconvection flow of MHD thixotropic nanofluid past a vertical surface coexisting with both nanoparticles and gyrotactic microorganisms. *Sci. Rep.* **2021**, *11*, 16627. [[CrossRef](#)] [[PubMed](#)]
36. Islam, S.; Ur Rasheed, H.; Nisar, K.S.; Alshehri, N.A.; Zakarya, M. Numerical Simulation of Heat Mass Transfer Effects on MHD Flow of Williamson Nanofluid by a Stretching Surface with Thermal Conductivity and Variable Thickness. *Coatings* **2021**, *11*, 684. [[CrossRef](#)]

37. Abderrahmane, A.; Qasem, N.A.A.; Younis, O.; Marzouki, R.; Mourad, A.; Chung, J.D. MHD hybrid nanofluid mixed convection heat transfer and entropy generation in a 3-D triangular porous cavity with zigzag wall and rotating cylinder. *Mathematics* **2022**, *10*, 769. [[CrossRef](#)]
38. Rehman, S.; Zeeshan; Rasheed, H.U.; Islam, S. Visualization of multiple slip effects on the hydromagnetic Casson nanofluid past a nonlinear extended permeable surface: A numerical approach. *Waves Random Complex Media* **2022**. [[CrossRef](#)]
39. Rasool, G.; Shah, N.A.; El-Zahar, E.R.; Wakif, A. Numerical investigation of EMHD nanofluid flows over a convectively heated riga pattern positioned horizontally in a Darcy-Forchheimer porous medium: Application of passive control strategy and generalized transfer laws. *Waves Random Complex Media* **2022**, 1–20. [[CrossRef](#)]
40. Nadeem, S.; Tumreen, M.; Ishtiaq, B.; Abbas, N.; Shatanawi, W. Second-grade nanofluid flow above a vertical slandering Riga surface with double diffusion model. *Int. J. Mod. Phys. B* **2022**, 2250237. [[CrossRef](#)]
41. Nadeem, S.; Ishtiaq, B.; Almutairi, S.; Ghazwani, H.A. Impact of Cattaneo–Christov double diffusion on 3d stagnation point axisymmetric flow of second-grade nanofluid towards a riga plate. *Int. J. Mod. Phys. B* **2022**, 2250205. [[CrossRef](#)]
42. Ishtiaq, B.; Zidan, A.M.; Nadeem, S.; Alaoui, M.K. Analysis of entropy generation in the nonlinear thermal radiative micropolar nanofluid flow towards a stagnation point with catalytic effects. *Phys. Scr.* **2022**, *97*, 085204. [[CrossRef](#)]
43. Nadeem, S.; Fuzhang, W.; Alharbi, F.M.; Sajid, F.; Abbas, N.; El-Shafay, A.S.; Al-Mubaddel, F.S. Numerical computations for buongiorno nano fluid model on the boundary layer flow of viscoelastic fluid towards a nonlinear stretching sheet. *Alex. Eng. J.* **2022**, *61*, 1769–1778. [[CrossRef](#)]